Proceedings of 8 ICSHMO, Foz do Iguaçu, Brazil, April 24-28, 2006, INPE, p. 235-243.

SEA-LEVEL PRESSURE PATTERNS IN SOUTH AMERICA AND THE ADJACENT OCEANS IN THE IPCC-AR4 MODELS

Alejandro Di Luca (1), Inés Camilloni (1)(2), Vicente Barros (1)(2)
(1) Departamento de Ciencias de la Atmósfera y los Océanos. FCEN. UBA
(2) Centro de Investigaciones del Mar y la Atmósfera (CIMA/CONICET-UBA)

1. INTRODUCTION

During the last years, many authors discussed low-level circulation changes both at regional and global scales. For example, at regional scale, some results show a southward shift of the South Atlantic high (Camilloni, 1999; Camilloni et al. 2005), a displacement to the south of the regional atmospheric circulation over Southeastern South America (Barros et al. 2000) and an enhancement of the easterly winds during the summer months over the Río de la Plata estuary (Simionato et al. 2005). These regional trends seem to be part of a more general hemispheric behaviour. Gibson (1992) showed a poleward shift of 3° of latitude on the maximum wind at 500 hPa in the 1976-1991 period. Van Loon et al (1993) calculated the latitude of the zonally averaged subtropical ridge over the Southern Hemisphere, finding a 2° trend over the 1976-1990 period. More recently, Gillett et al (2003) using outputs from four Global Climate Models (GCM) experiments found that the global pattern of the December-February sea level pressure (SLP) trends during the 1948-1996 period can be attributed to the growing global atmospheric concentration of greenhouse gases and sulphate aerosols. The SLP observed pattern shown by Gillet et al (2003) has predominantly positive trends at the 30º-45° latitude band of the Southern Hemisphere, and a trend of more than 2 hPa in the South Atlantic, off of the Argentine coast.

The objective of the present work is to evaluate the ability of a set of global climate models available for the preparation of the Fourth Assessment Report (AR4) of the Intergovernmental Panel on Climate Change (IPCC) to represent the predominant patterns of SLP over an extense region of the Southern Hemisphere that comprises Southern South America and the South Atlantic and South Pacific oceans. Additionally, those models with good representation of the dominant regional patterns were selected to analyze future scenarios. Predominant patterns of SLP and their evolutions were analyzed under two SRES scenarios. Differences between the forcing of these scenarios are mainly given in terms of atmospheric concentrations of greenhouse gases, ozone and aerosols.

(*) *Corresponding author address:* Alejandro Di Luca,
Dept. of Atmospheric and Oceanic Sciences. Univ. of Buenos Aires,
Cdad. Universitaria, Pabellón 2, (1428) Buenos Aires, Argentina.
E-mail: alejandrodiluca@gmail.com

2. DATA AND METHODOLOGY

This analysis is based on monthly mean SLP fields corresponding to NCEP/NCAR reanalyses and a set of GCMs over an area between 20°S-45°S and 130°W-0°. Two different periods were studied: one associated with present climate between 1978 and 2000, and the other associated with future climate, between 2001 and 2100. The relatively short period used to represent the present climate was selected because the reanalyses are more representative of real data over the oceanic areas only after 1978 when satellite data began to be fully used (Sturaro 2003).

The set of GCMs analyzed is available through the Program for Climate Model Diagnosis and Intercomparison (PCMDI) for the preparation of the IPCC-AR4. These models are coupled between ocean and atmosphere with different number of vertical levels in the atmosphere component which varies between 9 in CNRM-NM3 and 38 in UKMO-HadGEM1. The spatial resolution of this models varies between 1.25° and 4.0° in latitude and 1.875° and 5.0° in longitude. The evaluation of the simulations of present climate was done using Climate of the 20th Century (20C3M) experiments; the scenarios A1B and A2 were used for the period 2001-2100. Table 1 presents a list of the analyzed models, indicating the institution where it was generated, the name of the experiment, the number of available simulations and the corresponding period analyzed.

The identification of the dominant SLP patterns over the selected region was performed through a T-mode Varimax Rotated Principal Components Analysis (PCA) using the NCEP/NCAR reanalyses and the outputs from some selected models using the correlation matrix as input (Green et al.1978).

To evaluate the ability of the GCMs listed in Table 1 to represent the "observed" SLP fields, linear spatial correlation coefficients between monthly mean SLP fields derived from the NCEP/NCAR reanalyses and from GCMs were computed. Likewise, linear correlation coefficients between the PCs derived from the NCEP/NCAR reanalyses and from the GCMs outputs were calculated. Because of the different resolutions of the models, it was necessary to regrid SLP model outputs to the NCEP/NCAR reanalysis grid.

MODEL	INSTITUTION	EXPERIMENT		
		Climate of the 20th Century (20C3M)	SRES A2 experiment (850 ppm stabilization in 2100)	SRES A1B experiment (720 ppm stabilization in 2100)
CNRM-CM3 (1)	Météo-France / Centre National de Recherches Météorologiques FRANCE	1978-2000	2001-2100	2001-2099
CSIRO-Mk3.0 (1)	CSIRO Atmospheric Research AUSTRALIA	1978-1999	2001-2100	N/A
ECHAM5/MPI-OM (3)	Max Planck Institute for Meteorology GERMANY	1978-1999	2001-2100	2001-2099
GFDL-CM2.0 (1)	Geophysical Fluid Dynamics Laboratory UNITED STATES	1978-2000	2001-2100	2001-2099
GFDL-CM2.1 (1)	Geophysical Fluid Dynamics Laboratory UNITED STATES	N/A	2001-2099	2001-2099
GISS- EH (5)	NASA / Goddard Institute for Space Studies UNITED STATES	1978-2000	2001-2100	2001-2099
GISS-ER (5)		1978-2000	2001-2097	2001-2099
IPSL-CM4 (1)	Institut Pierre Simon Laplace FRANCE	1978-2000	2001-2100	2001-2099
UKMO-HadCM3 (2)	Hadley Centre for Climate Prediction and Research / Met Office UNITED KINGDOM	1978-1999	2001-2100	2001-2099
UKMO-HadGEM1 (2)		1978-1999	2001-2098	2001-2098

Table 1. List of GCMs. Number of available runs is indicated in brackets.

3. PRESENT PERIOD (1978-2000)

3.1 SLP variability for NCEP/NCAR

Figure 1 shows the three predominant SLP patterns obtained from the NCEP/NCAR reanalyses that explain almost 85% of the total variance. The first one (PC1) explains 43.2% of the variance and represents the summer surface circulation as suggests the seasonal contribution of these PCs presented in Table 2. This pattern has the South Atlantic and South Pacific highs in their southernmost position. The second (PC2) and third (PC3) patterns explain 27.3% and 14.1 % of the variance respectively and represent the winter circulation (Table 2). PC2 is characterized by the South Atlantic and South Pacific in the northernmost position and PC3 represents a surface pattern that it is dominated by the frontal activity during winter (Table 2).

	PC1	PC2	PC3
TOTAL	100.0	100.0	100.0
WINTER	7.7	**46.6**	**35.5**
AUTUMN	20.5	24.6	29.3
SPRING	28.0	22.3	22.1
SUMMER	**43.7**	6.5	13.2

Table 2. Seasonal contribution (%) to the total variance of the first three PCs.

The corresponding time series associated (factor loadings) with these three PCs are presented in Figure 2. These series show a positive linear trend for PC1 (summer mode), a slightly negative trend for PC2 (winter mode) and an almost null trend for PC3. These results indicate that the summer mode probably increased at the expense of the winter ones.

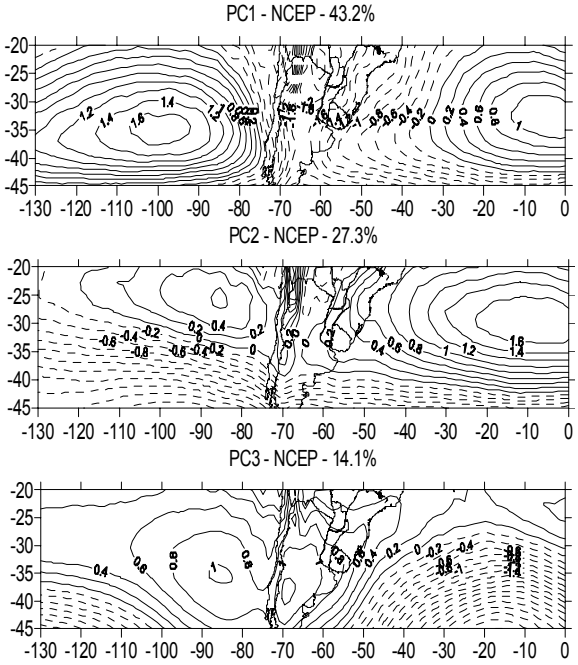

Figure 1. Principal Components of sea level pressure for NCEP/NCAR reanalysis

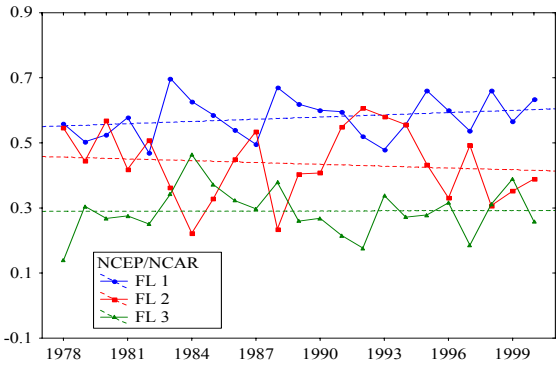

Figure 2. Factor loadings of the first three principal components.

3.2 GCMs regional validation for SLP

Figure 3 shows the monthly and annual linear correlation coefficients between SLP fields of one simulation of each GCM and the NCEP/NCAR reanalyses. All GCMs represent adequately the SLP fields during most of the year with the lower correlations during the austral autumn (March-April-May). The GCMs with better representation of the monthly mean SLP fields are UKMO_HadGEM1, UKMO_HadCM3, ECHAM5/MPI-OM, IPSL-CM4 and CNRM-CM3, with correlation coefficients higher than 0.75 for all months. Consequently, these GCMs were selected to identify the dominant SLP patterns and to compare them with the ones obtained with the NCEP/NCAR reanalyses.

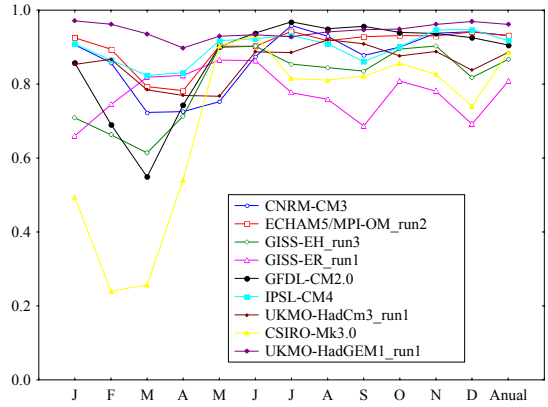

Figure 3. Spatial correlation coefficient between monthly mean SLP fields of the models and the NCEP/NCAR reanalvsis.

Figure 4 shows the SLP patterns obtained as a result of applying a Varimax Rotated PCA to the simulations of four GCMs: UKMO_HadGEM1, UKMO_HadCM3, ECHAM5/MPI-OM and CNRM-CM3. Results show that most of them represent the same dominant patterns. The explain variance varies from 41.8% to 45.8% for PC1, 28.4% to 34.8% for PC2 and 5.4% to 11.7% for PC3.

Temporal variability is also well represented, specially in UKMO_HadGEM1, ECHAM5/MPI-OM and CNRM-CM3 as these three GCMs represent the linear trends of the same sign as those obtained from the NCEP/NCAR reanalyses showing a slight increase of the summer mode at expense of the winter ones. Although UKMO-HadCM3 does not show a negative linear trend in PC2, the decrease of the winter mode could be explain by the negative trend in PC3.

Table 3 shows the contributiuons of the differents seasons to the explained variance of each PC. Results are similar to those of NCEP, mainly for PC1 and PC2. PC3 shows more variability within GCMs and in some of them it is asociated with spring and autumn seassons.

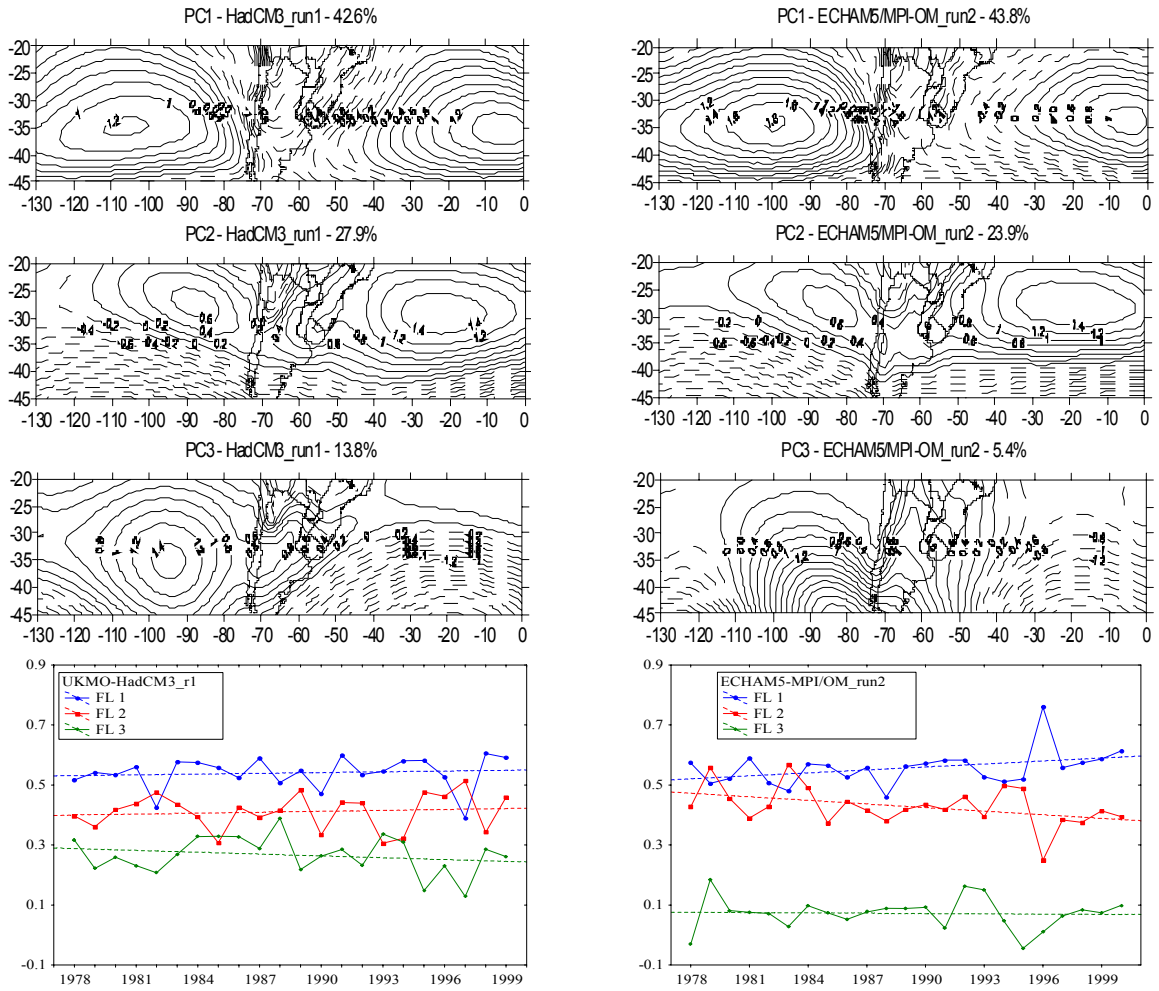

Figure 4. Principal components and factor loadings of SLP fields corresponding to UKMO-HadCM3 and ECHAM5/MPI-OM models for 20C3M experiments. Explained variance by each PC are also indicated.

20C3M EXPERIMENT						
	PC1	**PC 2**	**PC 3**	**PC 1**	**PC 2**	**PC 3**
	UKMO-HadGEM1 run1			**CNRM-CM3**		
TOTAL	100.0	100.0	100.0	100.0	100.0	100.0
WINTER	5.2	**54.4**	26.8	4.8	**45.6**	**39.8**
AUTUMN	26.4	19.4	24.2	17.9	31.6	25.8
SPRING	27.3	20.8	31.0	30.7	14.7	24.2
SUMMER	**41.1**	5.4	18.1	**46.5**	8.1	10.2
	UKMO-HadCM3 run1			**ECHAM5/MPI-OM run2**		
TOTAL	100.0	100.0	100,0	100.0	100.0	100.0
WINTER	2.9	**52.8**	**37.9**	3.9	**55.5**	26.2
AUTUMN	18.5	31.9	14.2	20.6	20.4	**38.9**
SPRING	30.0	11.6	41.1	32.0	20.0	19.6
SUMMER	**48.6**	3.6	6.8	**43.5**	4.1	15.3

Table 3. Seasonal contribution (%) to the total variance of the first three PCs. Largest values are indicated in red.

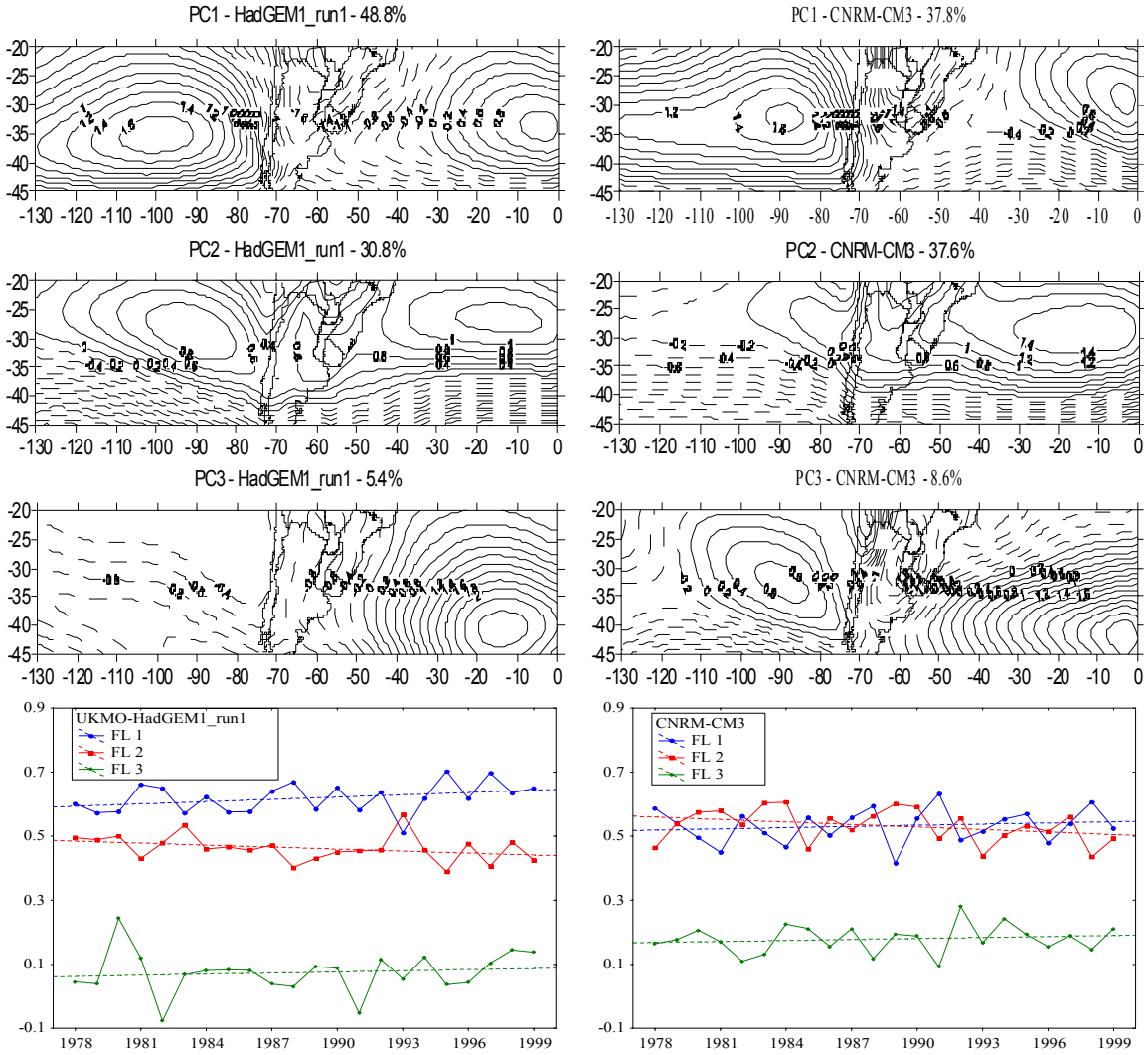

Figure 4 (cont.). For UKMO-HadGEM1 and CNRM-CM3 models.

Figure 5 shows the linear correlation coefficients between the PCs derived from the NCEP/NCAR reanalyses and from the GCMs outputs for the same models presented in Figure 3. All GCMs show correlation coefficients higher than 0.75 for the three factors with the exception of CNRM-CM3 and CSIRO-Mk3.0 in the third factor. The models with the best performance are the IPSL-CM4, GFDL CM2.0, UKMO-HadCM3 and ECHAM5/MPI-OM with correlation coefficients higher than 0.85 for all the factors.

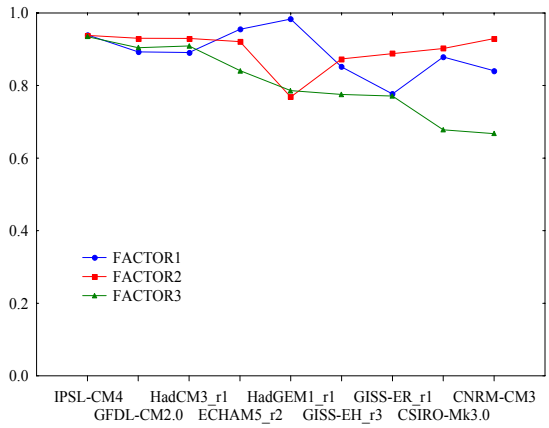

Figure 5. Linear correlation coefficients between PCs from NCEP/NCAR reanalyses and from GCMs outputs.

4. FUTURE SCENARIOS (2001-2100)

This section discusses the results obtained when applying a Varimax Rotated PCA to the GCMs outputs for scenarios A1B and A2. Only the GCMs with better agreement with the "observed" present climate represented by the NCEP/NCAR reanalyses were used.

Figure 6 shows the PCs and time series for the A1B scenario. Results derived for the A2 scenario are not shown as they are very similar to those obtained for the A1B. The patterns that characterize the first three PCs are approximately the same found for the 20C3M experiments and the explained variances by each PC are also similar to those found for the present period. PC1 varies between GCMs from 41.8 to 45.9%, PC2 varies from 28.4 to 34.8% and PC3 varies from 5.4 to 11.7%. Table 4 presents the seasonal contribution for the three PCs. The same patterns as in Table 3 are found, PC1 representing the summer circulation while PC2 represents the winter one. PC3 is mostly associated with different seasons except summer.

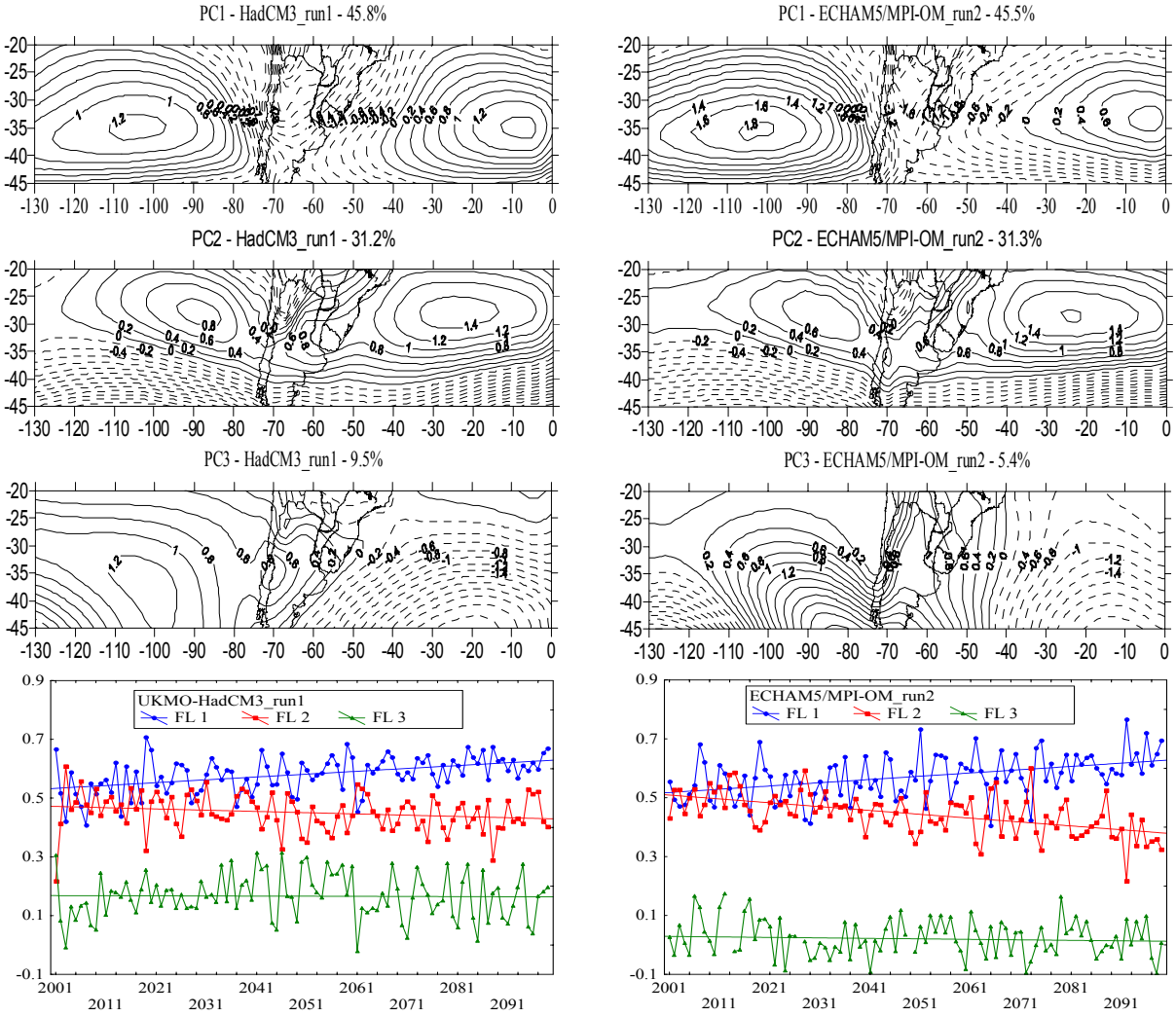

Figure 6. Principal components and factor loadings of SLP fields corresponding to UKMO-HadCM3 and ECHAM5/MPI-OM models for SRES A1B experiments. Explained variance by each PC are also indicated.

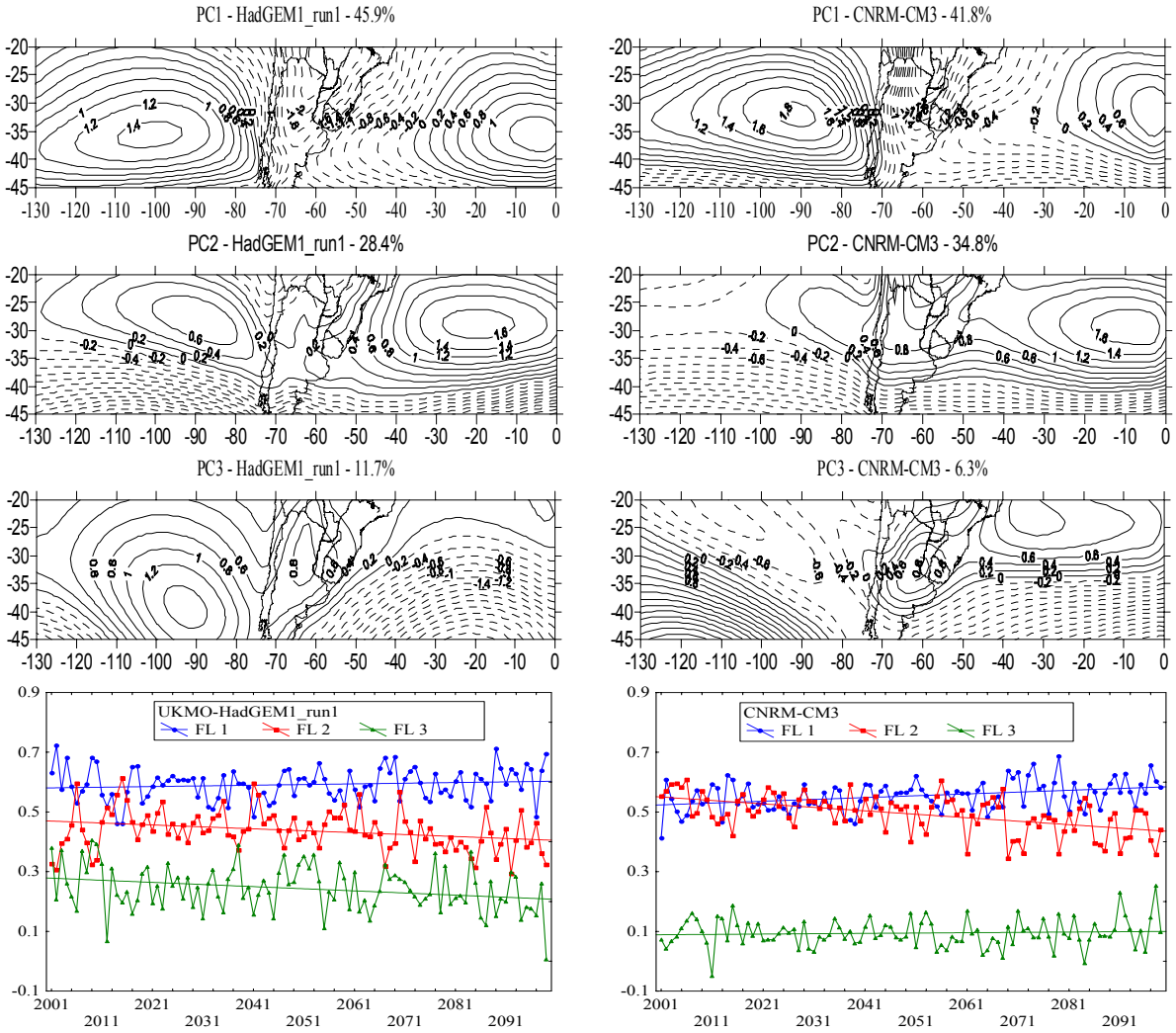

Figure 6 (cont.). For UKMO-HadGEM1 and CNRM-CM3 models.

SCENARIO A1B						
	PC 1	**PC2**	**PC 3**	**PC1**	**PC2**	**PC3**
	UKMO-HadGEM1 run1			**CNRM-CM3**		
TOTAL	100.0	100.0	100.0	100.0	100.0	100.0
WINTER	4.9	**52.3**	32.4	4.6	**50.2**	28.8
AUTUMN	23.4	20.2	32.8	10.4	34.5	19.9
SPRING	27.6	22.5	23.6	38.8	8.9	41.6
SUMMER	**44.3**	5.0	11.2	**46.1**	6.4	9.6
	UKMO-HadCM3			**ECHAM5/MPI-OM run2**		
TOTAL	100.0	100.0	100.0	100.0	100.0	100.0
WINTER	3.7	**55.0**	29.3	4.9	**53.2**	29.8
AUTUMN	20.4	27.4	17.8	20.2	24.3	32.1
SPRING	29.9	14.5	44.0	31.4	18.5	24.7
SUMMER	**46.0**	3.1	8.9	**43.4**	4.0	13.6

Table 4. Seasonal contribution (%) to the total variance of the first three PCs. Largest values are indicated in red.

The four GCMs show a positive trend for PC1 and a negative one for PC2, indicating an increase of the summer mode at the expense of the winter one. This behavior is repeated for all GCMs in the A1B and A2 scenarios although it is more pronounced in the A2 scenario. This result suggests that the calaculated trends depend on the differences between both forcings.
The differences between trends for both scenarios could be measure calculating the ratio between them:

$$R_i = \frac{PCT_i(A2)}{PCT_i(A1B)}$$

where PCT_i is the trend of PC_i. Results are presented in Table 5, showing that almost every GCM show larger trends of PC1 and PC2 for A2 scenario in comparison to A1B scenario.

	PC 1	PC 2
UKMO-HadCM3	1.40	2.75
CNRM-CM3	1.83	1.67
ECHAM5/MPI-OM	0.91	0.92
GFDL-CM2.0	1.27	1.55
UKMO-HadGEM1	4.00	2.33
GFDL-CM2.1	1.58	2.00
GISS-ER	1.18	0.16

Table 5. Ratio between PCs in scenarios A2 and A1B.

5. CONCLUSIONS

The T-mode PCA of the monthly mean SLP obtained from NCEP/NCAR reanalyses shows that there are three predominant patterns that characterize SLP fields over the extense region of the Southern Hemisphere that comprises Southern South America and the South Atlantic and South Pacific oceans. PC1 represents the summer surface circulation with the South Atlantic and South Pacific highs in their southernmost positions. PC2 and PC3 represent the winter circulation with the South Atlantic and South Pacific in the northernmost position (PC2) and a surface pattern that characterizes the frontal activity during that season (PC3). Temporal series of the three PCs show a positive linear trend of the summer mode and slightly negative trends for the winter indicating that the summer mode probably increased at the expense of the winter ones.
Monthly correlation coefficients between the output from the GCMs and the NCEP/NCAR reanalyses show that all of the models represent adequately the SLP fields during most of the year with the lower correlations during the austral autumn (March-April-May). The GCMs with better representation of the monthly mean SLP fields are UKMO_HadGEM1, UKMO_HadCM3, ECHAM5/MPI-OM, IPSL-CM4 and CNRM-CM3, with correlation coefficients higher than 0.75 for all months. Application of PCA to the GCMs outputs of four of these models show that most of them represent the same spatial and temporal varability identified with NCEP/NCAR reanalyses. These GCMs show the same three dominant patterns and also represent adequately the linear trends, showing an increase of the summer mode at expense of the winter ones, especially in UKMO_HadGEM1, ECHAM5/MPI-OM and CNRM-CM3. This result indicates that these set of GCMs are able to represent not only mean fields as shown in the spatial correlation analysis but also the interannual variability of SLP over the analyzed region.
The PCA performed to the GCMs output corresponding to the future period shows approximately the same predominant patterns of SLP obtained for the 20C3M experiments. The time series associated indicate that the increase of the summer mode at the expense of the winter one will continue. These trends are more pronounced in the A2 scenario showing that the changes could be related to differences between atmospheric concentrations gases.

Acknowledgments
This study was funded by the University of Buenos Aires under Grant X199, by the Agencia Nacional de Promoción Científica y Tecnológica under Grant PICT-07-14202 and IAI CRN-055.

6. REFERENCES

Barros V.; M.E. Castañeda and M.Doyle. 2000. Recent precipitation trends in Southern South America to the East of the Andes: an indication of a mode of climatic variability. In: Smolka P, Wolkheimer W (eds) Southern Hemisphere Paleo and Neoclimates Concepts, Methods, Problems. Springer, Berlin, 187-206.
Camilloni, I. 1999. Temporal variability of the Buenos Aires' urban heat island intensity. International Conference on Urban Climatology ICUC'99, Sydney Australia.
Camilloni, I.; V. Barros and A. Di Luca. 2005. Trends in the position of the South Altantic high and its representation by Global Climate Models: impacts over thr Río de la Plata estuary and adjacent ocean (in Spanish). Preprints of IX Congreso Argentino de Meteorología (CD-ROM). Buenos Aires, Argentina.
Gibson, T. 1992. An observed poleward shift of the Southern Hemisphere Subtropical wind maximum: A greenhouse symptom*?*. *Int. J of Climatol* **12**, 637-640

Gillett, N; F. Zwiers, A. Weaver and P. Stott. 2003. Detection of human influence on sea-level pressure. *Nature* **422**, 292-294.

Green, P. and E. Carol.1978. Analysing Multivariate Data. The Dryden Press. Illinois, USA, 519 pp.

Simionato, C.; C.Vera and F. Siegismund. 2005. Surface wind variability on seasonal and interannual scales over Río de la Plata. *J. of Coastal Research* **21**, 770-783.

Sturaro, G. 2003. A closer look at the climatological discontinuities present in the NCEP/NCAR reanalysis temperature due to the introduction of satellite data. *Climate Dynamics* **21**, 309-316.

Van Loon H, J. Kidson and A. Mullan. 1993. Decadal variation of the annual cycle in the Australian Data Sets. *J. of Climate* **6**, 1227-1231.